Journal of Power Sources 247 (2014) 26–31

Contents lists available at ScienceDirect

Journal of Power Sources

journal homepage: www.elsevier.com/locate/jpowsour

Electrochemistry of lithium–oxygen batteries using microelectrode voltammetry

E. Joseph Nemanick*

Energy Technology Department, The Aerospace Corporation, 2310 E. El Segundo Blvd., El Segundo, CA 90245, USA

HIGHLIGHTS

- Microcavity electrodes are a rapid tool for materials characterization.
- Li–O_2 discharge products are distinct species of surface and bulk Li_2O_2.
- Using single walled nanotubes leads to lower charge voltages and higher capacities.

ARTICLE INFO

Article history:
Received 30 May 2013
Received in revised form
29 July 2013
Accepted 16 August 2013
Available online 29 August 2013

Keywords:
Lithium–air
Lithium–O_2
Battery
Microelectrode

ABSTRACT

The electrochemistry of non-aqueous lithium–oxygen (Li–O_2) batteries on both reduction and oxidation was investigated using carbon black and single-walled nanotube (SWNT) microcavity electrodes. Two oxidative peaks were observed on oxidation (charge). The first peak at 3.0–3.7 V vs. Li/Li^+ was limited in storable charge ($\sim 8 \times 10^3$ C cm^{-3}). The oxidation potential of this first peak was independent of Li_2O_2 thickness (as measured by total charge on reduction) and assigned to interfacial Li_2O_2, lying between the bulk of the Li_2O_2 and the carbon surface. A second peak between 4.0 and 4.6+ V showed significant discharge product thickness dependence on oxidation potential and was assigned to bulk Li_2O_2, away from the carbon surface. On reduction (discharge), deposition of the interfacial Li_2O_2 showed a significant overpotential indicated by the ratio of interfacial/bulk Li_2O_2 formed at varying reduction potentials. SWNT were shown to effectively decrease the Li–O_2 average charge overpotential for a given charge by increasing the electrode surface area available for formation of interfacial discharge products.

1. Introduction

The energy storage capacity of intercalative materials such as layered oxides and carbons has begun to reach their practical limits and will be insufficient for the extended driving range required for mass adoption of electric vehicles as well as advancements in portable electronics [1]. To meet these needs, new battery chemistries are sought using next generation anode materials such as silicon and lithium metal, and group VI cathode materials sulfur [2,3] and oxygen [4,5] being the focus of extensive research. For oxygen, in particular, the reversible two electron reduction of O_2 in the presence of Li^+ to form Li_2O_2 in non-aqueous electrolytes has received considerable interest. Estimates for the energy density of practical systems range widely from 800 to 3000 Wh kg^{-1} [6,7], four to fifteen times the energy density of present Li-ion cells. Although this technology has the potential to offer significantly greater energy storage density than current Li-ion chemistry, there are significant issues related to oxygen electrode chemistry that must be addressed. Such issues as electrolyte breakdown [8], electrode reactivity [18,19], and high reaction overpotentials [9] are areas of intense research. A complete understanding of the oxygen reduction reaction (ORR) and oxygen evolution reaction (OER) mechanisms in reversible non-aqueous aprotic electrolytes remains elusive.

Recent work [10] has eliminated the previous solvents of choice, alkyl carbonates, as suitable for Li–O_2 due to their decomposition to form Li_2CO_3 with cycling. Analysis of evolved gas using differential electrochemical mass spectrometry, DEMS [11], as well as Fourier transform infrared spectroscopy (FTIR) [12], Raman spectroscopy [13], and nuclear magnetic resonance (NMR) [14] studies have shown that reduced O_2 species react with alkyl carbonates rather than reversibly cycling [15]. Attention has since been focused on etheric solvents [16] such as dimethoxy ethane (glyme) and tetraglyme which while still showing some oxidative instability at high potentials [17], does reversibly produce Li_2O_2 on the cathode. Reports also indicate that these highly reduced O_2 species may also

* Tel.: +1 (310) 336 0093.
E-mail addresses: ejoseph.nemanick@aero.org, nemanice@gmail.com.

0378-7753/$ – see front matter © 2013 Elsevier B.V. All rights reserved.
http://dx.doi.org/10.1016/j.jpowsour.2013.08.043

react with the high surface area carbon materials used as electrodes, which may call for investigation of more oxidatively stable high specific surface area materials [18–20].

Understanding the nature of the oxygen reduction reaction (ORR) and oxygen evolution reactions (OER) is fraught with difficulty. Several models have been advanced after the semi-reversible reaction of oxygen with lithium was discovered in etheric solvents [9,21,22]. Many measurements have characterized Li–O_2 reaction chemistry using macroscale (>1 mm) electrode cycling and/or rotating disk [9] (or ring disk [23]) measurements. Macroscale measurements give fidelity to end use, but are necessarily slow and can contain many confounding elements. The rotating electrodes eliminate effects from slow diffusion rates and low O_2 solubilities at the expense of using representative electrode materials, as they rely on Pt and glassy carbon disks. It is critical to develop techniques to allow for evaluation and elucidation of the fundamental reaction mechanism without other processes such as diffusion, Li anode degradation, and solution impedance and capacitance, while still using end-product relevant electrode materials.

To study the ORR and OER processes, this project has utilized microcavity voltammetry. Microcavity voltammetry uses a pore formed by etching back the wire of a metal microelectrode packed with high surface area electrode material. Microcavity electrodes, like microelectrodes, increase the mass transport of oxygen to the electrode through hemispherical diffusion, but also use the same electrode materials as their macroscale cousins. Microcavity electrodes cannot be strictly modeled using conventional microelectrode equations, for in addition to the hemispherical diffusion of species to and from the cavity opening, there is a diffusion process down the length of the cavity through the porous material, and so acts like a hybrid of micro- and macro-electrodes. Current passing through the small working electrode surface is greatly reduced, decreasing the *i*R losses associated with the organic electrolyte and increasing the usable scan rates. The small surface area also reduces the capacitive signal of the electrode, allowing the Faradaic signal to be more easily measured. In addition, the small absolute amount of Li^+ consumed during cycling allows for the substitution of a non-lithium counter electrode, removing the confounding effects of a highly reactive electrode from the measurements.

2. Experimental

2.1. Preparation of active material

For studies of carbon electrode lithium–oxygen cells, the high surface area carbon electrode was made from Super C65 carbon black (Timcal, BET surface area 62 $m^2\ g^{-1}$), with a particle size distribution between 30–50 nm. In addition, single walled carbon nanotubes (SWNT, 1.4 nm dia., 1/3 conducting:2/3 semiconducting, NanoIntegris, ~1000 $m^2\ g^{-1}$) were also tested as higher surface area materials. Carbon black or SWNT (100 mg) in *iso*-propanol (5 mL) were sonicated in a MiSonix S-4000 Ultrasonicator at 17 W for 10 min to disperse the carbons. 10% dry weight of T-30 Teflon water-based emulsion (DuPont) was added and the solution was mixed. The *iso*-propanol and water were then evaporated under an active vacuum. The dried material was then formed into a thick gum by addition of small amounts of *i*-propanol and thoroughly mixed and folded until the material was uniform. Microcavity electrodes were fabricated adapting a technique from Wang et al. [24]. A 15 μm Pt wire microelectrode (Ametek, Berwyn, PA) was polished flat using 0.1 μm alumina, and then immersed in hot (80 °C) aqua regia for 30 min to etch down the Pt wire and form a microcavity. Active material was then worked into the microcavity by using the electrode as a pestle against a glass surface. The cavity filling was observed by microscope and the excess material removed by cleaning with a soft cloth. The electrode was then dried in vacuum before use. At the end of experimentation, the active material was removed from the cavity by sonicating in *i*-propanol and the electrode was freshened by dipping in room temperature aqua regia for <5 s before refilling and reuse.

2.2. Electrochemical measurements

Electrochemical measurements were carried out with either 0.5 M tetrabutylammonium trifluoromethane sulfonate (TBATFS, Aldrich, >99.0%) or 0.5 M lithium trifluoromethane sulfonate (triflate, LiTFS, 99.995%, Aldrich) in diglyme (DG, anhydrous, 99.5% Aldrich, dried over molecular sieves), prepared in an Ar glovebox. Lithium triflate was chosen as the salt due to its slightly better stability on cycling and lower charge voltage plateau than the imide salt, LiTFSI. The reference electrode was a Ag wire, isolated from the working electrode by a Vycor frit, in 10 mM $AgNO_3$/0.5 M LiTFS/DG. The reference electrode was kept ~1 cm from the working electrode. The 10 mM Ag/Ag^+ reference electrode was 3.52 V [10] more positive than a Li/Li^+ reference, which was not used as the presence of O_2 can cause variations in the reference potential of this electrode. For some studies, the LiTFS was replaced with the TBATFS, to examine the chemistry in the absence of Li^+. O_2 free electrolyte measurements were performed in an Ar glovebox (O_2 < 1 ppm, H_2O < 1 ppm) with an electrolyte prepared from solvent and salt stored in the glovebox. A three electrode cell was prepared using 20 mL of 500 mM LiTFS or TBATFS in DG in a dried three neck flask with a stainless steel mesh counter electrode (2 × 2 cm). For O_2 saturated experiments, the solution was bubbled with O_2 (Matheson, 99.997%, passed over a $CaSO_4$ drying column) with vigorous stirring for 1 h. The O_2 saturation of the solution was tested by watching for a change in reductive response to vigorous stirring or direct bubbling of O_2 over a test electrode surface during a galvanostatic scan. If the current during reduction did not increase, the solution was deemed to be saturated. The potentiostat was a PAR 273A run using Corrware software.

3. Results and discussion

3.1. Microelectrode voltammetry

Typical voltammograms of microelectrodes for a reaction with freely diffusing reactants and products show a profile similar to high rate rotating systems, with the typical peak of macroscale cyclic voltammograms (CVs) being replaced with a steady state saturation current and little reaction hysteresis [25]. For non-aqueous lithium–oxygen chemistry in glymes the solid product Li_2O_2 formed from the ORR occludes the surface and prevents subsequent reaction reducing the saturation current and eventually terminating the reaction [9,16,21,22]. Fig. 1 shows a CV of 15 μm diameter × 30 μm deep cavity carbon black electrode scanned at 10 mV s^{-1} in (A) O_2 free and (B) O_2 saturated 0.5 M LiTFS electrolyte in DG. These traces can be compared to the same electrode in (C) O_2 saturated, Li^+ free, 0.5 M TBATFS/DG. Both O_2 saturated samples (with and without Li^+) showed the onset for the ORR, starting at ~2.7 V vs. Li/Li^+ for the LiTFS and ~2.2 V for TBATFS, demonstrating the stabilization of reduced oxygen species by Li^+ in forming Li_2O_2 [26,27]. The overall reaction of

$$2Li^+ + O_2 + 2e^- \rightarrow Li_2O_2\,(s) \quad (1)$$

forms an insoluble, poorly conducting product which slowly decreases the active surface area. The electrically insulating nature of the discharge product will retard subsequent reduction. As the thickness of discharge products increases, reduction at the surface

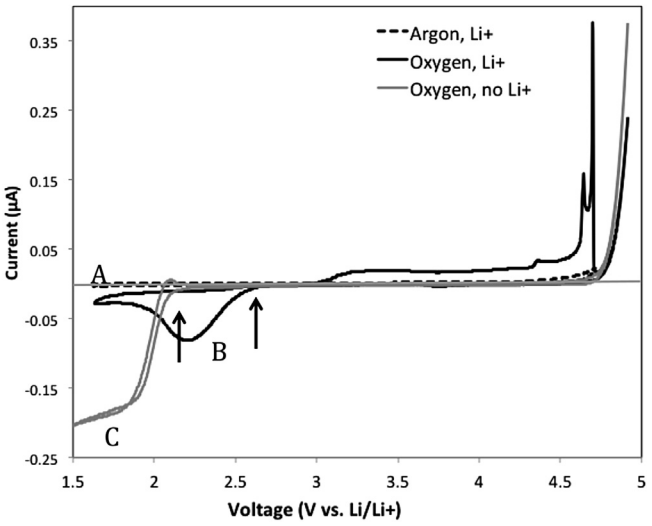

Fig. 1. Cyclic voltammograms of 15 μm dia. carbon black electrode in diglyme in (A) Ar in LiTFS, (B) LiTFS saturated in O_2, and (C) in TBATFS saturated with O_2 at 10 mV s^{-1}. With Li^+ the ORR comes to a halt as the surface is covered by discharge products, while with TBA^+, and without Li^+ the ORR shows no current loss or hysteresis before the O_2 diffusion limit. The arrows mark the onset of the reduction reactions for (B) and (C).

slows and eventually stops, leading to a decline in current which causes the formation of a peak that looks superficially similar to a diffusion controlled peak. Although similar in shape to a diffusion controlled peak, instead of running out of diffusing reactant, the electrode runs out of active surface area. This is similar to galvanostatic discharges where the discharge potential decreases to the experimental limit as the electrode runs out of capacity as the entire surface becomes occluded with discharge products. In Fig. 1 reduction of O_2 with Li^+ showed a peak and decline of the reductive current while with TBA^+ it showed a more typical microelectrode reaction with little hysteresis in the curve and a near saturation of current at the O_2 diffusion limit that increased only slightly due to background processes. The reduction in the surface area can also be seen in the difference in the maximum reductive currents. The same electrode with Li^+ showed a maximum O_2 reduction current less than in TBA^+, indicating that formation of Li_2O_2 on the surface prevented the electrode from reaching the O_2 diffusion limited current. This indicates that for this scan rate the discharge reaction was not diffusion limited, but rather surface limited.

While the O_2 reduction with TBA^+ showed the OER reaction as a very small oxidative peak at ~2.1 V due to residual reduced species, most of the reduced oxygen diffused away from the electrode and was not available for oxidation. The only other oxidative signal in TBATFS was the positive solvent window starting at ~4.6 V, similar to that seen in LiTFS. In contrast to this, the O_2 reduced with Li^+ showed the onset of oxidation starting at ~3.0 V and a broad peak centered at ~3.5 V, and one or two very sharp peaks at 4+ V. The scan was extended out to the solvent window to capture all discharge product oxidation. The bi/trifurcation of the second oxidation peak was ascribed to spontaneous formation of O_2 bubbles which irregularly interrupts the current flow but does not disrupt to total charge passed. Typically for these microelectrodes, the amount of integrated charge on oxidation was ~85% of the charge on reduction. This high parity between discharge and charge indicates that almost all of the oxidative reactions were included in this extended scan window. The 4+ V peak can be difficult to observe as this peak shifts to higher oxidative potentials depending on the thickness of deposited material and scan rate. It can easily shift above the solvent window, as will seen in Fig. 4. In addition to this thickness dependent peak shift, if the electrolyte was not kept rigorously dry, the 4+ V peak broadens and shifts to ~3.7 V, and merges into the edge of the 3.5 V peak.

3.2. Assignment of Li_2O_2 discharge products

Fig. 2 shows successive cyclic voltammetric scans of a carbon electrode saturated in O_2 with LiTFS from 100 mV s^{-1} to 2.5 mV s^{-1}. At 100 mV s^{-1} significant reduction continued even as the potential sweeps positive, and continues up to the reduction onset potential. By 50 mV s^{-1}, the reverse scan on reduction no longer had much reductive current. On oxidation, the 3.5 V peak was very significant in current at the higher scan rates, and declined in relative magnitude with decreasing scan rate. Plotting the peak height of the 3.5 V peak vs. scan rate (Fig. 3a), it can be seen that the peak height is linear with scan rate, as opposed to the square root of the scan rate, which indicates the OER was not a diffusion limited reaction under these conditions for this oxidation process. This was expected, as the reactant Li_2O_2 is a solid, and thus should not diffuse and show diffusion controlled oxidation. However, on reduction, the current fell off above 100 mV s^{-1}, which is indicative of a reaction that cannot keep up with the faster scan rates either from slow diffusion of O_2 to the surface or slow reaction kinetics. To evaluate the relative amounts of the separate charge reactions, the area under the peaks was integrated, from 3.0 to 3.8 V for the 3.5 V peak, and from 3.8 to 4.75 V for the 4+ V peak. The total integrated charge (Fig. 3b) under the 3.5 and 4+ V peaks shows that the 3.5 V oxidation does not increase much with scan rate and plateaus at 10 mV s^{-1} and slower, while the 4+ V peak continues to increase in total charge. This indicates that the oxidation at 3.5 V was of a fixed amount of discharge products, regardless of scan rate on reduction, with a capacity of 8×10^3 C cm^{-3} of carbon black. The oxidation of discharge products at 4+ V did not show a charge limit under these conditions, indicating that quantity of material to be oxidized increased with increasing time spent reducing (slower scan rates). Because these two discharge products are not in a fixed ratio, they do not appear to be the successive oxidation of a single reactant, i.e. A → B → C but rather the oxidation of two electrochemically distinct species.

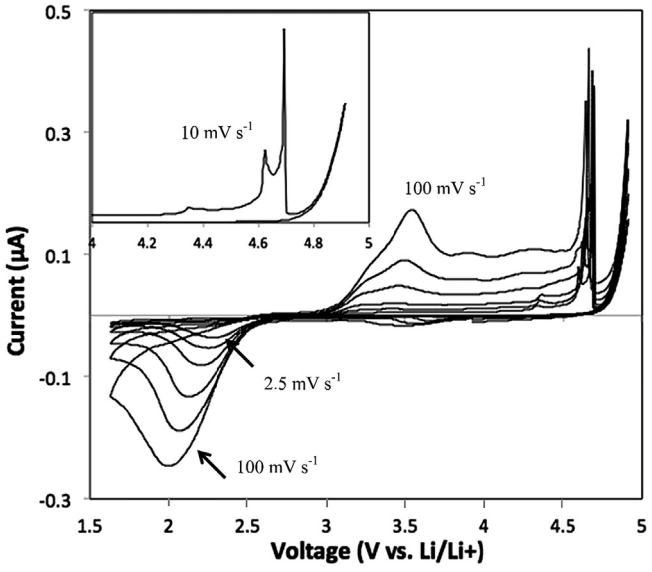

Fig. 2. Successive scan rates ranging from 2.5 to 100 mV s^{-1} for carbon in LiTFS saturated with O_2. Inset is the 10 mV s^{-1} scan for the charge peak, showing the bi/trifurcation of the peak. This peak splitting was ascribed to spontaneous nucleation of O_2 bubbles temporarily disrupting the current flow.

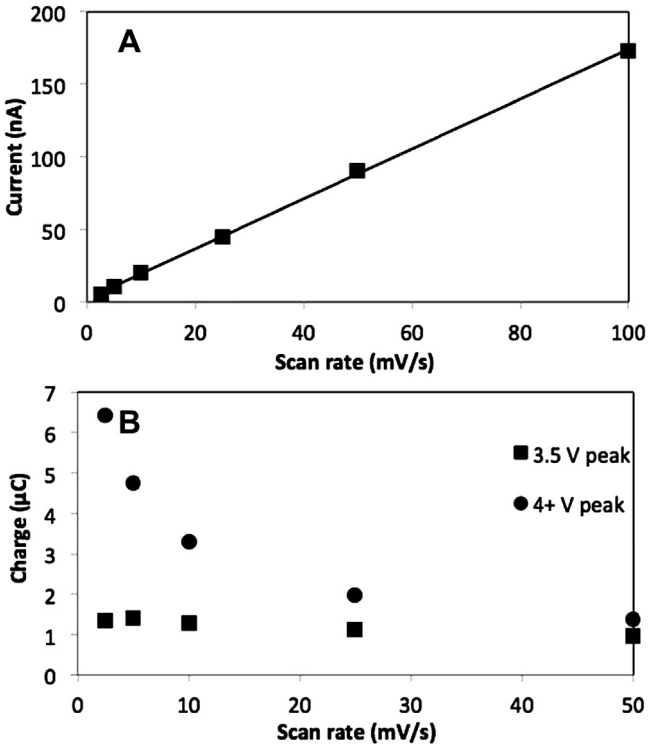

Fig. 3. A) Scan rate dependence of anodic peak height for the 3.5 V peak, showing a linear trend with scan rate, indicating a surface bound reaction. B) Shows the total integrated charge for the 3.5 and 4+ V peaks, showing a finite capacity of the 3.5 V peak. The dividing line for integration was chosen as 3.8 V.

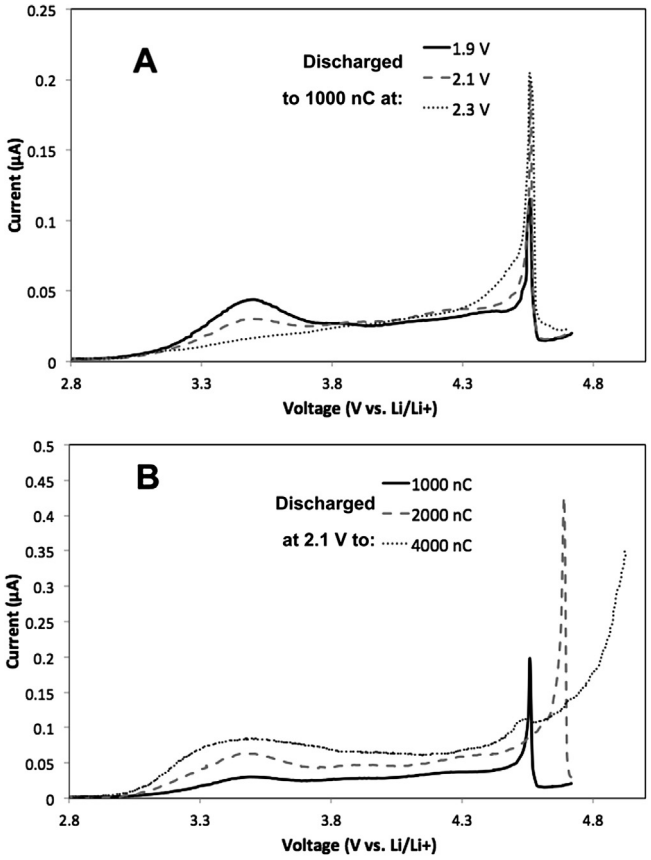

Fig. 4. Charge voltammograms after a potentiostatic discharge. A) The oxidation of an electrode discharged potentiostatically at 2.3, 2.1, and 1.9 V. The reduction for each was limited to 1000 nC. The ratio of interfacial Li_2O_2 to bulk Li_2O_2 shifted favoring bulk at milder reducing potentials. B) After potentiostatically discharging at 2.1 V to 1000, 2000, and 4000 nC, this voltammogram shows that despite the increasing thickness of discharge products, the oxidation potential of the interfacial Li_2O_2 was unaffected, while the bulk Li_2O_2 oxidation potential increased due to *i*R effects.

Potentiostatic reduction of O_2 shows how the relative population of these two discharge species are dependent on the discharge conditions. Fig. 4a shows the oxidation of an electrode that was potentiostatically discharged to a fixed charge, and therefore a fixed quantity of discharge products. These discharges were at three different potentials, 2.3, 2.1, and 1.9 V. As the reduction potential became more negative, the ratio of product oxidizable at 3.5 V to that oxidizable above 4 V increases. Fig. 4b shows the thickness dependence of the oxidation potentials for these two species. As the total charge (and thus thickness of deposited materials) was increased from 1000 nC to 4000 nC at a constant reductive potential, the relative proportions of 3.5 V:4+ V species was unchanged. The 4+ V oxidation was strongly shifted to higher potentials as the thickness increased while the 3.5 V species was unaffected.

Combining the results of both Figs. 3 and 4, it can be seen that the discharge products oxidizing at 3.5 V have a limited capacity and their oxidation potential does not shift with material thickness. In contrast, the 4+ V material had a far greater discharge capacity, but had an oxidation potential that continued to increase as material thickness increased, suggestive of an *i*R shift due to a low conductivity material.

As put forth previously [28], the two discharge products can be assigned to two electrochemically separate species, bulk Li_2O_2, and an interfacial Li_2O_2 that lies at the boundary of the carbon electrode and the bulk Li_2O_2. Though the discharge process for this particular experimental setup did not show multiple peaks on reduction, indicating the reduction currents significantly overlapped, their distinct oxidation properties allows for this assignment. Li_2O was ruled out as the species represented by the 4+ V peak due to previous studies [29] using Li_2O pre-filled electrodes not evolving O_2 at these potentials in glymes, as well as DEMS studies not showing the minimum $4e^-$ per O_2 molecule evolved required by the oxidizing species being Li_2O as opposed to Li_2O_2 [26].

The oxidative distinction between the discharge products into interfacial Li_2O_2 directly in contact with the carbon surface and bulk Li_2O_2 has been seen elsewhere [30], where chemically prepared Li_2O_2 mechanically mixed with carbon black to form the electrode does not show the 3.5 V peak, but only the 4+ V peak. In addition, recent studies [31] of very thin (<0.7 nm, ~2 atomic layers) Li_2O_2 have shown that the oxidation reaction starts at very low overpotentials of ~200 mV, or 3.2 V vs. Li/Li+, similar to the beginning of the interfacial Li_2O_2 oxidation peak. Density Functional Theory (DFT) calculations [32] have shown that the oxygen rich surfaces of Li_2O_2 are relatively depleted in electrons compared to bulk Li_2O_2 and should have a lower oxidation potential in addition to being more conductive. The Li_2O_2 at the bulk Li_2O_2/carbon interface should be expected to oxidize preferentially over the bulk, and with a lower overpotential. Furthermore, as Fig. 4b depicts, the oxidation potential of interfacial Li_2O_2 did not shift with increasing amount of material deposited, while the second peak (assigned to bulk Li_2O_2) shifts to ever more positive potentials as material thickness increased, thus indicating that there was likely an *i*R component to the oxidation of this material.

The separation of discharge materials can also bee seen in the nucleation overpotential for their formation. As the potentiostatic reduction overpotential was increased in Fig. 4a, the quantity of interfacial over bulk Li_2O_2 increased, indicating that there was an overpotential required for the formation of the Li_2O_2 on the carbon surface. Deposition of Li_2O_2 on an electrode surface during

discharge has been proposed to start from a nucleation site with subsequent growth occurring preferentially on Li_2O_2 surfaces [33,34], and has been observed previously in TEM with the formation of large balls of Li_2O_2 on the electrode surface as opposed to a conformal coating in some conditions [30,31]. Interfacial Li_2O_2 in this study oxidized prior to the bulk material, indicating that oxidation proceeds from the electrode surface outward into the bulk. This has been seen in these TEM studies where on charge the Li_2O_2 was observed to oxidize starting from the electrode/Li_2O_2 interface.

Recent studies of isotopically labeled carbon electrodes [18,19] have suggested that a layer of Li_2CO_3 forms on the surface of the carbon cathode during cycling. At least half of the Li_2CO_3 comes from reaction of discharge products with the etheric electrolyte, and the other half possibly coming from oxidation of the carbon electrode. Differential electrochemical mass spectroscopy (DEMS) studies monitoring gas production during oxidation do not show significant CO_2 production in the 3.5 V region on charge [18], indicating that the oxidation peak assigned above to interfacial Li_2O_2 is unlikely to be dominated by Li_2CO_3 decomposition. Any layer of insulating Li_2CO_3 on the surface of the electrode should hinder interfacial Li_2O_2 oxidation. Since the Li_2O_2 still does oxidize and produce O_2 it would seem to indicate that either the carbonate layer is discontinuous, with the measured activity of the electrode being the areas not covered by Li_2CO_3, or that the carbonate layer is thin enough to not substantially affect the oxidation of the Li_2O_2. Some part of the current in the 4+ V oxidation peak may be due to carbonate oxidation as opposed to the OER, as DEMS showed a sharp increase in CO_2 at these potentials. However, fractional monolayers of carbonate salts from surface oxidation should not show a progressive shift in oxidation potential with increasing thickness of discharge products as seen in Fig. 4b. In addition, the 4+ V CO_2 production in the DEMS study was not associated with a current, indicating that it was not consistent with the electrochemical oxidation observed herein.

The surface controlled aspect of the interfacial Li_2O_2 was also demonstrated by examining a higher surface area carbon material, single-walled nanotubes (SWNT), which had more than ten times the surface area of the carbon black. Fig. 5a shows a voltammogram of a SWNT electrode compared to a carbon black electrode in O_2 saturated LiTFS. SWNT electrodes showed a greater volumetric charge storage capacity than carbon black electrodes, as well as a larger fraction of this charge stored in the interfacial, surface bound products. SWNT electrodes had a larger fraction of the discharge product oxidation occurring in the 3.5 V regime, with relatively less material oxidizing above 4+ V as seen in Fig. 5b. The relative fraction of the oxidation ascribed to interfacial Li_2O_2 was greater with the higher surface area SWNT, and did not saturate at these scan rates as was seen for the carbon black surfaces. This indicates that for this particular configuration of the cell, there was insufficient oxygen supplied during reduction to fully use the SWNT electrode surface as can be seen in the linearity of plot of the peak height for interfacial Li_2O_2 oxidation vs. the square root of the scan rate v. This linearity with respect to $v^{1/2}$ of peak height for the

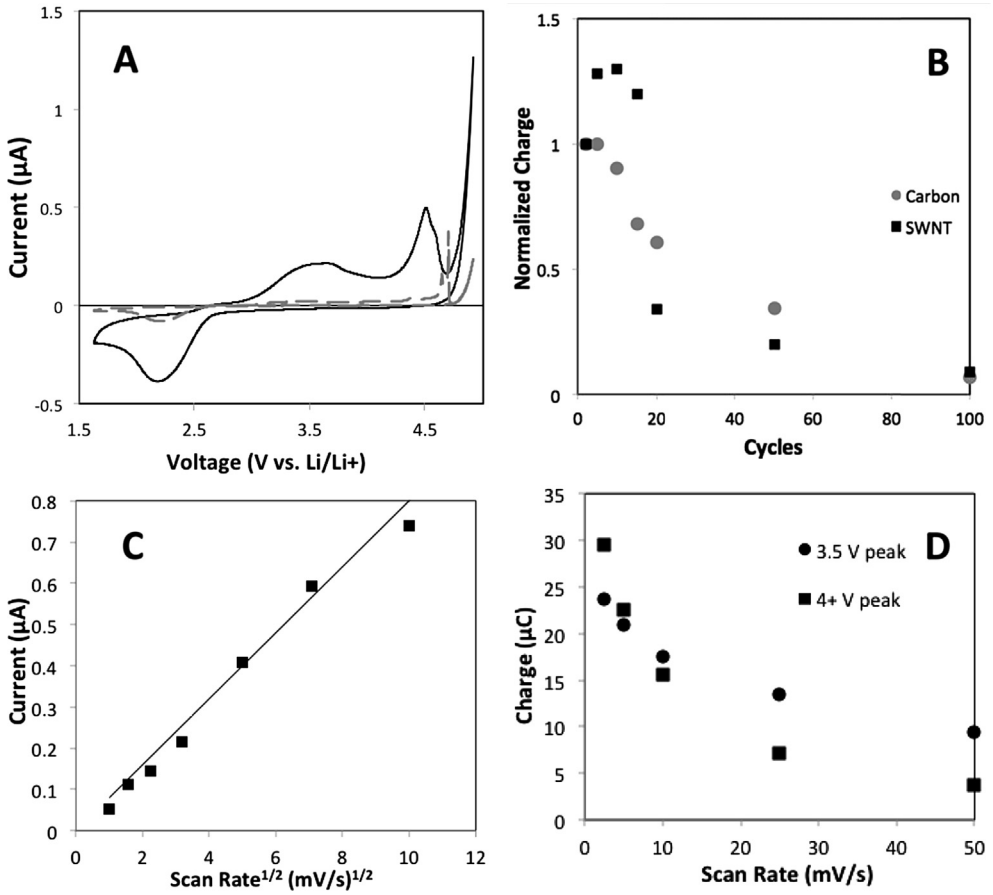

Fig. 5. A) CV of SWNT (black) and carbon black (gray) at 10 mV s^{-1} in LiTFS saturated in O_2. B) The total normalized charge for 100 cycles at 10 mV s^{-1} for carbon and SWNT electrodes. C) A Randles–Sevcik like plot for the oxidation of interfacial Li_2O_2 on SWNT, showing the linear trend up to mV s^{-1}. D) A plot of the charge under each oxidation peak for SWNT, indicating there was insufficient oxygen to saturate the surface of the electrode.

oxidation reaction (as a proxy for the ORR which did not allow for separation of interfacial and bulk Li_2O_2 formation) indicates that the discharge product formation was diffusion limited as opposed to what was seen for the carbon black electrodes in Fig. 3a. Presumably, with a sufficiently slow discharge, or sufficiently high O_2 transport using a smaller microelectrode, these SWNT electrodes would exhibit similar properties to the carbon black electrodes with non-diffusion limited products. However, this would require far more O_2 than even this microelectrode setup is capable of supplying.

Increasing the surface area of the electrode using SWNT not only increased the charge storage capability, it also reduced the charge potential for a given capacity by making the lower overpotential surface bound Li_2O_2 the dominant form of the stored charge. In addition, the capacity of SWNT electrodes falls off similarly to the carbon black electrodes, as seen in Fig. 5b. If a partial monolayer of Li_2CO_3 was formed from electrode oxidation, then the capacity of SWNT electrodes ought to be seen to decompose much faster than for carbon black electrodes as the single layer carbon material should be far more sensitive to loss of activity due to oxidation than the much larger carbon black particles, indicating that oxidation of SWNT is not a rapid process.

4. Conclusion

It has been shown here that the ORR produces two electrochemically distinct Li_2O_2 species that can be differentiated by their behavior on charge. The interfacial layer of Li_2O_2 formed on reduction is bound directly to the carbon surface and has a significant overpotential for formation, but has a low oxidation overpotential on charge, occurring between 3–3.7 V. It does not show a rate dependence on its oxidation potential from *i*R effects due to its close proximity to the electrode. A second Li_2O_2 layer is formed on the surface of this nucleated Li_2O_2, and oxidizes at higher potentials, ~4–4.6 V, and its oxidation potential shifts with charge rate and thickness of deposited material. As this material is not strictly limited to the finite surface of the electrode, it stores the majority of the charge during cycling. The relative amounts of interfacial and bulk Li_2O_2 can be manipulated by increasing the reductive potential on discharge as well as by increasing the surface area using SWNT, both of which effectively reduce the overpotential on charge.

Acknowledgments

The author gratefully acknowledges The Aerospace Corporation's Independent Research and Development (gs1) program for funding, and Dr. Don Walker for SWNT electrode supply.

Appendix A. Supplementary data

Supplementary data related to this article can be found at http://dx.doi.org/10.1016/j.jpowsour.2013.08.043.

References

[1] J.M. Tarascon, M. Armand, Nature 414 (2001) 359–367.
[2] D. Peramunage, S. Licht, Science 261 (1993) 1029.
[3] X. Ji, K.T. Lee, L.F. Nazar, Nat. Mater. 8 (2009) 500.
[4] K.M. Abraham, Z. Jiang, J. Electrochem. Soc. 143 (1996) 1.
[5] J. Read, J. Electrochem. Soc. 149 (2002) A1190.
[6] P.G. Bruce, S.A. Freunberger, L.J. Hardwick, J.M. Tarascon, Nat. Mater. 11 (2012) 19–29.
[7] J. Christensen, P. Albertus, R.S. Sanchez-Carrera, T. Lohmann, B. Kozinsky, R. Liedtke, J. Ahmed, A. Kojic, J. Electrochem. Soc. 159 (2012) R1–R30.
[8] V.S. Bryantsev, F. Faglioni, J. Phys. Chem. A 116 (2012) 7128–7138.
[9] Y.C. Lu, H.A. Gasteiger, Y. Shao-Horn, J. Am. Chem. Soc. 133 (2011) 19048.
[10] Y.C. Lu, H.A. Gasteiger, E. Crumlin, R. McGuire Jr., Y. Shao-Horn, J. Electrochem. Soc. 157 (2010) A1016–A1025.
[11] M.M.O. Thotiyl, S.A. Freunberger, Z. Peng, P.G. Bruce, J. Am. Chem. Soc. 135 (2013) 494.
[12] F. Mizuno, S. Nakanishi, Y. Kotani, S. Yokoishi, H. Iba, Electrochemistry 78 (2010) 403.
[13] B.D. McCloskey, D.S. Bethune, R.M. Shelby, G. Girishkumar, A.C. Luntz, J. Phys. Chem. Lett. 2 (2011) 1161–1166.
[14] S.A. Freunberger, Y. Chen, Z. Peng, J.M. Griffin, L.J. Hardwick, F. Barde, P. Novak, P.G. Bruce, J. Am. Chem. Soc. 133 (2011) 8040.
[15] M. Leskes, N.E. Drewett, L.J. Hardwick, P.G. Bruce, G.R. Goward, Angew. Chem. Int. Ed. 51 (2012) 8560.
[16] J. Read, J. Electrochem. Soc. 153 (2006) A96.
[17] K.R. Ryan, L. Trahey, B.J. Ingram, A.K. Burrell, J. Phys. Chem. C 116 (2012) 19724–19728.
[18] B.D. McCloskey, A. Speidel, R. Scheffler, D.C. Miller, V. Viswanathan, J.S. Hummelshoj, J.K. Norskov, A.C. Luntz, J. Phys. Chem. Lett. 3 (2012) 997–1001.
[19] W. Xu, J. Hu, M.H. Engelhard, S.A. Towne, J.S. Hardy, J. Xiao, J. Feng, M.Y. Hu, J. Zhang, F. Ding, M.E. Gross, J.G. Zhang, J. Power Sources 215 (2012) 240–247.
[20] Y.C. Lu, Y. Shao-Horn, J. Phys. Chem. Lett. 4 (2013) 93.
[21] S.H. Oh, L.F. Nazar, Adv. Eng. Mater. 2 (2012) 903–910.
[22] H.J. Jung, J. Hassoun, J.B. Park, Y.K. Sun, B. Scrosati, Nat. Chem. 4 (2012) 579–585.
[23] J. Herranz, A. Garsuch, H.A. Gasteiger, J. Phys. Chem. C 116 (2012) 19084–19094.
[24] Y. Wang, D. Zheng, X.Q. Yang, D. Qu, Energy Environ. Sci. 4 (2011) 3697–3702.
[25] I. Montenegro, M.A. Queiros, J.L. Daschbach, Microelectrodes: Theory and Applications, Springer, 1991.
[26] B.D. McCloskey, R. Scheffler, A. Speidel, G. Girishkumar, A.C. Luntz, J. Phys. Chem. C 116 (2012) 23897–23905.
[27] V.S. Bryantsev, Theor. Chem. Acc. 131 (2012) 1250–1261.
[28] E.J. Nemanick, in: Electrochemical Society Fall Conference, 2012.
[29] N. Tsiouvaras, S. Meini, I. Buchberger, H.A. Gasteiger, J. Electrochem. Soc. 160 (2013) A417–A477.
[30] S.H. Oh, R. Black, E. Pomerantseva, J.H. Lee, L.F. Nazar, Nat. Chem. 4 (2012) 1004.
[31] Y.C. Lu, E.J. Crumlin, G.M. Veith, J.R. Harding, E. Mutoro, L. Baggetto, N.J. Dudney, Z. Liu, Y. Shao-Horn, Sci. Rep. 2 (2012) 1–6.
[32] M.D. Radin, J.F. Rodriguez, F. Tian, D.J. Siegel, J. Am. Chem. Soc. 134 (2012) 1093–1103.
[33] J.S. Hummelshoj, J. Blomqvist, S. Datta, T. Vegge, K.S. Rossmeisl, K.S. Thygesen, A.C. Luntz, K.W. Jacobsen, J.K. Norskov, J. Chem. Phys. 132 (2010) 071101-1–071101-4.
[34] J.S. Hummelshoj, A.C. Luntz, J.K. Norskov, J. Chem. Phys. 138 (2013) 034703-1.